Reduced Graphene Oxide-SnO$_2$-Polyaniline Ternary Composite for High-Performance Supercapacitors

**VIMUKTHI JAYAWEERA*[1,3], W.L.N.C. LIYANAGE[2],
R.C.L. DE SILVA[1], S.R.D. ROSA[2] and IRESHA R. M. KOTTEGODA[1]**

[1]Materials Technology Section of Industrial Technology Institute,
No. 363, BauddhalokaMawatha, Colombo 07, Sri Lanka.
[2]Department of Physics, University of Colombo, Colombo 03, Sri Lanka.
[3]Sri Lanka Institute of Nanotechnology (SLINTEC), Mahenwatta,
Pitipana, Homagama, Sri Lanka.

Abstract

A novel symmetric supercapacitor electrode material, rGO-SnO$_2$-polyaniline nanocomposite, was synthesized using graphite oxide, SnCl$_2$.2H$_2$O, and pure Aniline as precursors in a scalable and straightforward one-pot process. Analysis revealed that the rGO-SnO$_2$-polyaniline composite had been successfully synthesized. When the two-electrode supercapacitor was assembled using 1M H$_2$SO$_4$, it showed an outstanding specific gravimetric capacitance of 524.2 F/g at a 5 mV/s scan rate. To the best of our knowledge, such a higher value for a two-electrode specific capacitance for a supercapacitor was never reported. Furthermore, even at a high current density of 1 A/g, the material disclosed an outstanding charge-discharge characteristic. Thus, the rGO-SnO$_2$-polyaniline nanocomposite could also be used as an electrode for commercial supercapacitors.

Introduction

Rapid development in electric/hybrid vehicles and portable electronic devices in the modern world had created a higher demand for energy storage devices. Electrochemical capacitors (ECs) or super capacitors have great world wide attention due to the advantages mainly for their high power density, short charge-discharge time, and long cycle life.[1,2] There are three primary electrode materials used in supercapacitors: carbon-based materials, transition metal oxides, and conductive polymers. Transition metal oxides are the best candidate for ECs with higher specific capacitance and meager resistance resulting in higher specific power. Graphene or

reduced graphene oxide (rGO) is an excellent electronic conductor with a higher theoretical specific surface area, higher chemical stability, and excellent mechanical properties.[3–5] Graphene-based hybrid materials are used to develop double-layer capacitors. SnO_2-based nanocomposite with a 7:1 mass ratio of NiO and SnO_2 has been shown a maximum specific capacitance of 464 F/g at 5 mV/s, suggesting its potential as an electrode material for high energy density commercial supercapacitors.[6] SnO_2 based electrode materials are inspiring due to their high theoretical specific capacitance, simple synthesis process, low cost, and low toxicity.[7,8] Conducting polymers such as polyaniline (PANI) and polypyrrole (PPy) are widely studied for supercapacitors because of their low cost, strong electrochemical activity, and satisfactory electrochemical stability.[9] Synthesis of ternary hybrid material, combining three main categories of electrode materials, may reduce their downsides. Researchers have successfully created novel ternary nanocomposites with high capacitance and long stability for batteries and supercapacitors.[7,10–12] The properties of an EC depends on the electrode material, the electrolyte, as well as the cell design. The capacitance values for respective composites strongly depend on the cell construction. In the case of three-electrode cells, extremely high specific capacitances are reported,which vary from 250 to 3105.46 F/g for different material combinations.[13,14] However, for two-electrode cells, much smaller specific capacitances have been reported,such as 20 F/g for symmetrical cells with two α-MnO_2 electrodes,[15] 225 F/g for nitrogen-doped porous carbon fiber at 1 A/g,[16] and 360 F/g for PANI/ MWCNTs.[17] Predicted specific gravimetric capacitance for monolayer graphene-based on its theoretical specific surface area (2630 m^2/g) is a significantly higher value (~550 F/ g), despite reported gravimetric capacitance for both aqueous and organic electrolytes are less than 200 F/g for single component graphene derivatives which is typically due to the poor quality of the graphene material and lowering specific surface area due to restacking or poor exfoliation.[18] Two- and three-electrode systems have been chosen to study the electrochemical characteristics of SnS_2 nanorods. The specific capacitance of nanorods displayed 270 F/g at 10 mV/s and 162.2 F/g at 3 A/g. However, SnS_2/rGO system diminishes the aqueous hybrid supercapacitor's specific capacitance to 108 F/g at 5 mV/s and 92.4 F/g at 1 A/g.[19] Three-electrode parameters help to determine the electrochemical properties of the materials.

Nonetheless, a two-electrode test cell simulates the physical structure, internal voltages, and charge transfer in a packaged architecture of a practical supercapacitor.[20] Understanding the EC's real performance is critical in developing a commercial EC, which has received little attention. As a result, the current research focuses on the construction and analysis of a two-electrode device. Furthermore, developing free-standing graphene-based materials as supercapacitor electrodes can increase electrochemical performance and attract attention.GSP nanocomposite can be produced in situ using graphene oxide and a one-pot scalable method. When producing graphene oxide (GO), Sri Lankan graphite was utilized because of its great purity. On the graphene basal plane, $SnCl_2$ is used to reduce GO while concurrently creating SnO_2. A two-electrode configuration was designed to evaluate the material's performance as a full-scale, commercial supercapacitor.

Methodology
Materials
Natural Graphite with a purity of 99.9% was obtained from Kahatagaha Graphite Lanka (Ltd), Sri Lanka. All other chemicals were used in this experiment were analytical grade, and Aniline is double distilled before use.

Synthesis of Graphene/ SnO_2/Polyaniline (GSP) Composite
A graphite oxide (GO) suspension was prepared by dissolving 400.0 mg of dry GO powder in distilled water as previously reported method.[21, 22] 3.00 g of $SnCl_2$.$2H_2O$ was added to the GO suspension while stirring and sonication for 3 h. In this process, $SnCl_2$ is used to reduce GO and concurrently produced SnO_2 on the surface of graphene, and the by-product HCl formed in the solution changing the pH during the process.[23] The reaction mixture showed a color change from light brown to black after 1.5 h sonication. The pH value was set to 1.5 by adding drops of NH_3. Thereafter, 3.9 ml of Aniline was added to the solution while the solution was in an ice bath, and temperature is maintained at 4-6°C during the process. Finally, 9.78 g of $(NH_4)_2S_2O_8$ was added slowly into the solution, where the color of

the solution turned blackish green. The final mixture was stirred for 24h and centrifuged at 3900 rpm for 12 minutes to decant the supernatant. The remaining solid material was washed with distilled water three times followed by one time with ethanol, and dried at 60ºC for 12 h to remove moisture.

Fabrication of GSP Electrochemical Supercapacitor

Firstly, 80 wt% GSP composite, 10 wt% acetylene black (carbon black N-330), and 10 wt% Polyvinylidene fluoride (PVDF) dissolve in N-Methyl-2-Pyrrolidone (NMP) is mixed to compose a slurry paste for the preparation of electrodes. The resulting paste was applied on two stainless steel electrodes (1.0 cm^2), and each electrode contains 1.00 mg of the active material. Then the electrodes were placed in a vacuum oven at 60 °C for 2 h. Finally, both positive and negative electrodes are separated using a paper separator containing the 1M H_2SO_4 as electrolyte. The electrode assembly holds tightly in the prepared test cell, as shown in Fig.1a and Fig.1c.

Fig.1: (a) Test cell with two stainless steel electrodes (b) Prepared electrodes for testing (c) Final supercapacitor assembly

Material Characterization

X-ray powder diffraction (XRD) analysis was conducted to identify the crystalline phase composition of the prepared GSP composite at the range of 5º–80º with Cu Kα1 radiation (λ = 1.5406 Å) at 40 kV and 40 mA using Regaku Ultima IV X-ray diffractometer. A LEO 1420vp scanning electron microscope was used to examine the morphology of the GSP composite scanning electron microscope (SEM). Functional groups attached to Graphite oxide and GSP composite were characterized using a BRUKER Tenor 27 FTIR-ATR spectrometer. The Raman spectra were obtained using a Bruker Senterra II Raman Microscope excited at 532 nm green laser. X-ray photoelectronic spectroscopy (XPS) analysis was performed with a Thermo Scientific TM ESCALAB Xi+spectrometer. Cyclic voltammetry (CV), charge-discharge cycles, and electrochemical impedance spectroscopy (EIS) were performedusing Biologic SP-150 potentiostat. EIS measurements were tested in between 1 mHz to 1 MHz frequency range, and impedance curves were analyzed with the EC-Lab V10.40 software. The electrochemical testing was carried out using a two-electrode test cell constructed as in Fig. 1.

Results and Discussion

It is important to verify the formation of rGO-SnO$_2$-PANI composite (GSP) through various analytical techniques such as XRD, FTIR, SEM, XPS, Raman before investigating the performance of GSP composite as a supercapacitor. In this work, several instrumental analyses were used to verify the composite and explore the physical and chemical characteristics.

X-Ray Diffraction (XRD) Analysis

XRD analysis is carried out to characterize the crystallinity and phase purity of GSP composites.[24] Figure 2 (a,b) shows XRD spectra of GO and the GSP composite, respectively. In Fig.2a, the strong peak observed at 2θ = 9.66° for GO confirmed

that graphite is wholly converted to GO during the synthesis of GO from graphite.[22] The XRD main peak corresponds to graphite generally appeared at about $2\theta = 26°$ which is completely disappeared in the spectra due to oxidation of graphite. Fig.2b shows the XRD patterns for GSP. Since rGO is formed upon reduction of GO, during the synthesis of the composite, the XRD main peak corresponding rGO should also be appeared at about $2\theta = 26°$ in Fig 2b.[22] Although it is not seen presumably overlaps with another peak at the same position as shown below. The diffraction peak ascribed to the (1 1 0), (1 1 1), (2 1 1), and (301) planes of tetragonal rutile

SnO_2 is detected for the GSP composite at 2θ about 26.7°, 33.6°, 51.8°, and 65.9° respectively. Certain peaks are not seen due to low intensities,and the low intense broad peaks indicate that the SnO_2 particles have a low degree of crystallinity and small crystallite size. The average crystalline size (D) of the SnO_2 of the GSP composite as determined using the Debye–Scherrer equation from the strongest (110) plane diffraction peak ($2\theta = 26.7$) is about 28.4 nm.[25,26] The XRD analysis suggests complete oxidation of Sn^{2+} to Sn^{4+} with the reduction of GO to rGO, even though the formation of rGO is verified through some other techniques, as shown later.
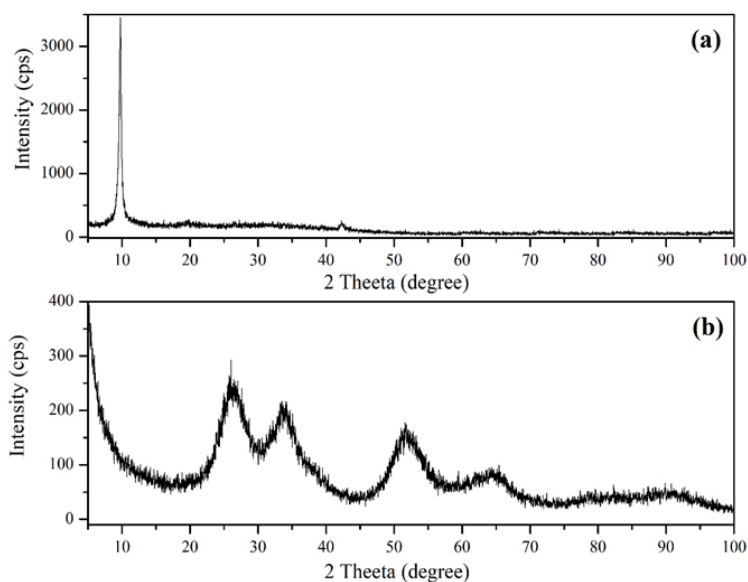

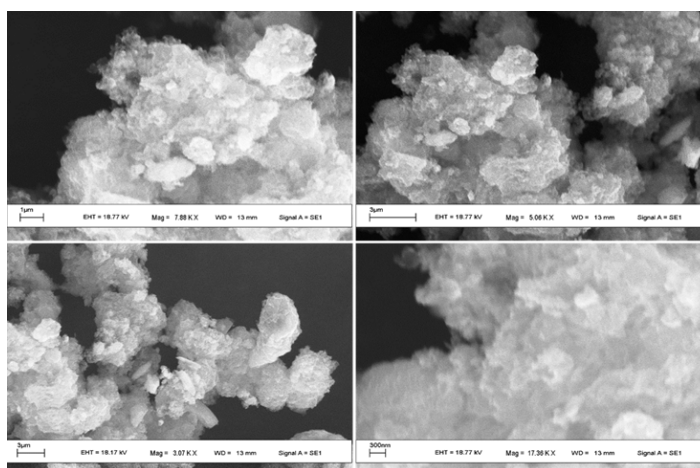**Fig. 2: X-ray powder diffraction (XRD) patterns of (a) GO (b) GSP Composite**

Fig. 3: Scanning Electron Microscopy (SEM) images of the GSP composite

Scanning Electron Microscopy (SEM)

The surface morphology and microstructure of the GSP composite were investigated through scanning electron microscopy (SEM).[24] Although the presence of Graphene or rGO is not clear in the image, the aggregates of particles are attributable to SnO_2 nanoparticles attached to rGO. This kind of morphology gives a higher surface area, and the surface area is proportional to the capacitance due to larger double-layer capacitance leading to higher specific capacitance.

Fourier Transform Infrared Spectroscopy (FTIR)

Although the presence of rGO and PANI is not detected fully through both XRD and SEM analysis, the FTIR spectra of the GSP composite[24] shown in Fig.4 reveals a peak at 1638 cm^{-1} associated with stretch vibrations of the C=N bond of PANI. The small shoulder at 1249 cm^{-1} and peak at 3228 cm^{-1} is ascribed to C-N starching vibrations. The strong peaks at 1485 cm^{-1} and 1568 cm^{-1} are assigned to C=C stretching of benzenoid rings and C=C stretching of the quinonoid rings of PANI and rGO.[27] The peak at 1057 cm^{-1} and a sharp peak at 1288 cm^{-1} assign to C-O stretching primary alcohol and C–O stretching of epoxide groups remain in rGO, and the low band around 792, 879 cm^{-1} corresponds to C-H bending and band 2000-1900 cm^{-1} C=C stretching of rGO. Meanwhile, the peaks present at 554 cm^{-1} and 595 cm-1 are characteristic vibration modes of O-Sn-O and Sn-O, which indicates the formation of SnO_2. Even though some vibrations are common to PANI and the rGO, the FTIR data show that the rGO-PANI-SnO_2 composite was successfully formed.
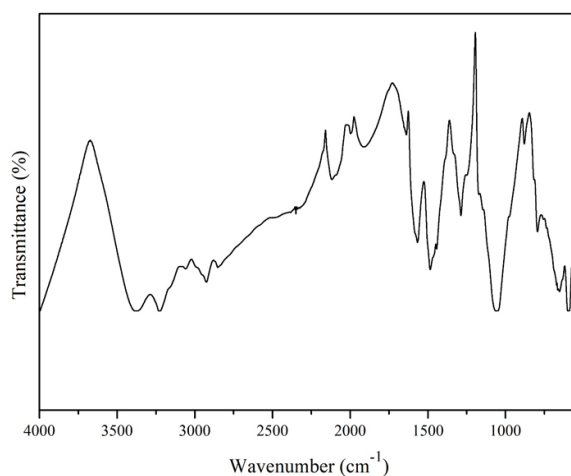
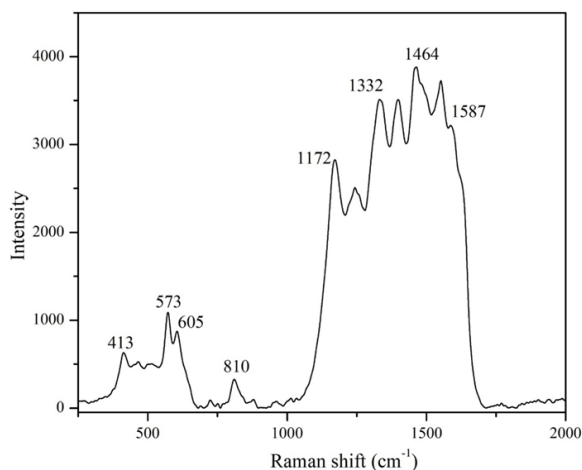

Fig. 4: FTIR spectra of the GSP composite

Fig. 5: Raman spectra of the GSP composite

Raman Spectroscopy

Raman spectroscopy is a powerful non-destructive technique to study the vibrational modes of molecules present in graphene and its composites. Raman spectroscopy of GSP composite is shown in Fig.5. The peak at around 1332 cm^{-1} (D-band) is related to the defects and disordering of the hexagonal structure. The 1587 cm^{-1} peak (G-band) is due to the vibration of sp2-bonded carbonatomsin a 2D hexagonal lattice representing the rGO, indicating the successful reduction of GO. The broadband around 2600-3200 cm^{-1} means the 2D band of rGO,the second-order of the D band.573,

and 605 cm^{-1} Raman modes are the fingerprint of the oxygen vacancies in SnO_2 crystal structures.[28] The Raman peaks also confirm the formation of PANI at 413, 810, 1172, 1243, 1399, 1464, and 1552 cm^{-1}.[29] Hear, the C=C stretching vibrations of the quinonoid rings appear in 1552 cm^{-1}, and 1243, 1399, 1464 cm^{-1} are attributed to the C–N stretching in quinonoid structures highly localized platonic structures, and C=N stretching vibrations in quinonoid units represent respectively. The Raman analysis verifies the presence of each material in the GSP composite and the nature of the bonding.
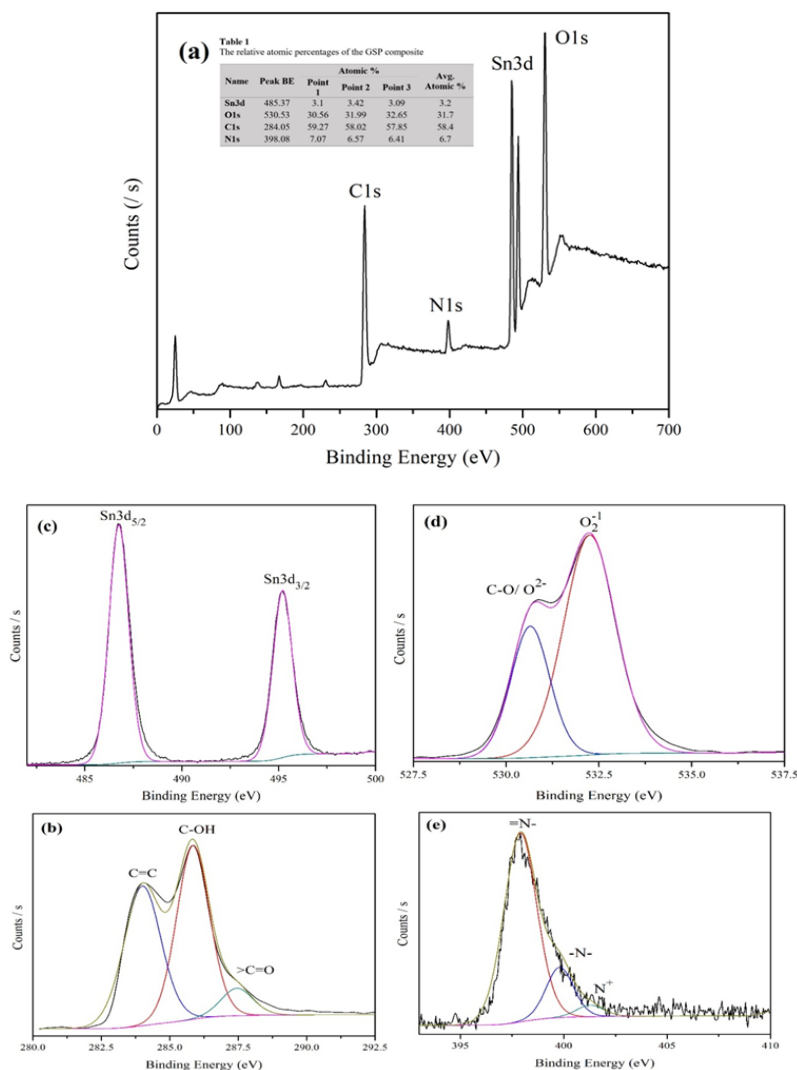

Fig. 6: (a) XPS spectra of the GSP composite (b) The deconvoluted C1s spectra (c) The deconvoluted Sn3d spectra (d) The deconvoluted O1s spectra (e) The deconvoluted O1s spectra (Inset: Table 1 - Relative atomic percentage of GSP composite)

X-ray Photoelectron Spectroscopy (XPS) Analysis

The XPS analysis is also useful to identify materials and their composition in addition. Accordingly, the presence of rGO, SnO_2, and PANI is validated by the XPS as well. Fig. 6 a shows the XPS survey scan of the GSP composite. The proportion of the GSP composite is calculated from the relative atomic percentages of C, N, O, and Sn in the GSP composite scan at three different points. The corresponding photoelectron peak areas are listed in Table 1 (inset of figure 6). Fig.6b shows the narrow scan of C1s, the native Graphene peak at 284.05 eV, which is ordinary sp^2 carbon atoms in aromatic rings, confirming the existence of rGO. The long tail to higher binding energies is due to hydroxyl (C–OH) groups attached to the carbon at 285.85 eV and carbonyl (>C=O) groups at 287.45 eV. The formation of SnO_2 from $SnCl_2$ is clearly illustrated in Fig.6c; the peak at 486.75 eV is ascribed to the $3d_{5/2}$ of Sn^{+4}, the peak at 495.2 eV to the $3d_{3/2}$ of Sn^{+4}, and the peak at approximately 24.1 eV to the Sn $4d_{5/2}$.[30] Figure 6d shows a narrow scan of O1s spectra at 532.25 eV and 530.65 eV, corresponding to oxygen absorption (O_2^-) or oxygen bonded to aliphatic carbon(C–O) and oxygen binding (O^{2-}) due to the rGO as well as SnO_2. The narrow scan of N1s shown in Fig. 6e, the peaks corresponding to quinoid di-imine nitrogen (=N–), benzenoid diamine nitrogen (–NH–), and protonated imine (N+) appear at 397.9 eV, 399.8 eV, and 401.27 eV is attributable to the PANI.
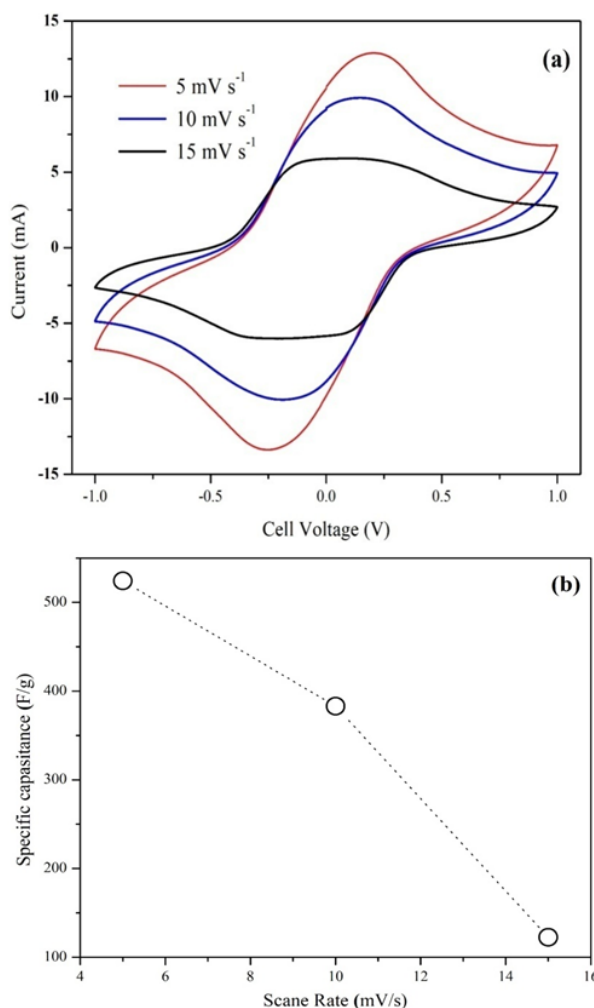

Fig. 7: (a) Cyclic voltammetry response at different voltage scan rates,
(b) Variation of specific capacitance function of voltage scan rate

Electrochemical Characterization

Cyclic voltammetry (CV), charge-discharge cycles, and electrochemical impedance spectroscopy (EIS) were carried out to evaluate the electrochemical performance of the synthesized GSP composite using two-electrode configurations. Figure 7a shows CV graphs at different scan rates within -1 V to +1 V operation voltage window.The highest specific capacitance observed was 524.2 F/g at a 5 mV/s scan rate which is a considerably high value for the two-electrode system. *In-situ* formation of SnO_2 on rGO has resulted in good charge transfer among interconnection of nanoparticles resulting in high capacity. The above argument is confirmed by impedance analysis, as shown later. As shown in Fig.7b, the specific capacitance is decreased when the scan rate is increased. This performance is attributable to charge-transfer resistance affecting

at high rate charge-discharge. The CVs of the ideal capacitor performs with rectangular like shape. However, this exemplary behavior is distorted with a gradual loss in cell-specific capacitance upon increasing the scan rate. This phenomenon is typical for all supercapacitors, reflecting the limited mass transfer kinetics within the porous electrode layer.

The electrochemical performance was further studied using galvanostatic charge/discharge under different current densities such as 1 A/g, 2 A/g, and 3 A/g within the voltage limits +1 V and -1 V as shown in Fig.7b. The degradation of a supercapacitor is also studied through charge-discharging the cell over many cycles (~1500 cycles); Figure 8a depicts a portion of a charge-discharge cycle. Throughout, modest variations in specific capacitance and equivalent series resistance were noted.
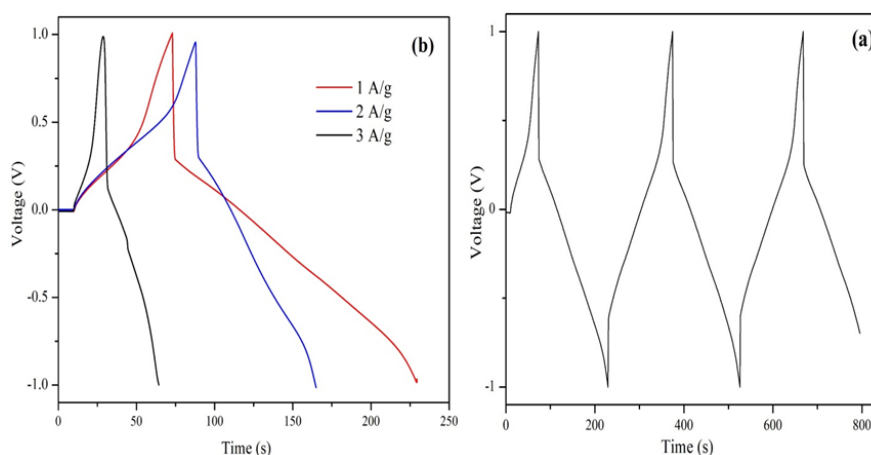

Fig. 8: (a) Galvanostatic charge-discharge cycles at 1 A/g current density. (b) Galvanostatic charge/discharge under different current densities

The charge-discharge curves obtained are nearly linear and symmetric, revealing an excellent capacitive behavior. Charging-discharging cycle time is reduced when the current density is increased. Even in a high current density at 1 A/g, cycle time shows a better discharging time of 230 sec. The IR drop of the charge-discharge cycle in Fig.8b also varies with the discharge current density, and equivalent series resistance (R_{esr}) is estimated using $\Delta V = 2IR_{esr}$ and value is 0.3532 Ω/g for current density at 1 A/g due to voltage drop of 0.7065 V.

EIS measurements are obtained from the frequency range of 1 mHz to 1 MHz,and the impedance curves

are analyzed using EC-Lab V10.40 software. Fig.9 shows the Nyquist plot and the equivalent circuit constructed for the two-electrode cells. The equivalent series resistance (R_{esr}) is 1.091Ω, the charge transfer resistant (R_{ct}) is 2.434 Ω, the parallel leakage resistance (R_p) is 246.2 Ω, and the double-layer capacitance (C_{dl}) is 24.57 μF. Pseudocapacitance is 0.8658 F leading to a specific capacitance of 494.7 F/g, and the value is comparable with the specific capacitance recorded as 524.2 F/g from the CV data showing the capacitive nature of the ternary composite material. The last element is called the Warburg element (W), which is the diffusion impedance of electrolyte, which

is 1.739 $\Omega/s^{1/2}$. Although the values R_{ct} and R_{esr} are relatively low, the cell shows much higher parallel leakage resistance (R_p), which is responsible for the radius of the hemisphere. The lower conductivity of the stainless steel current collector is believed to give higher parallel leakage resistance, which is to be improved.
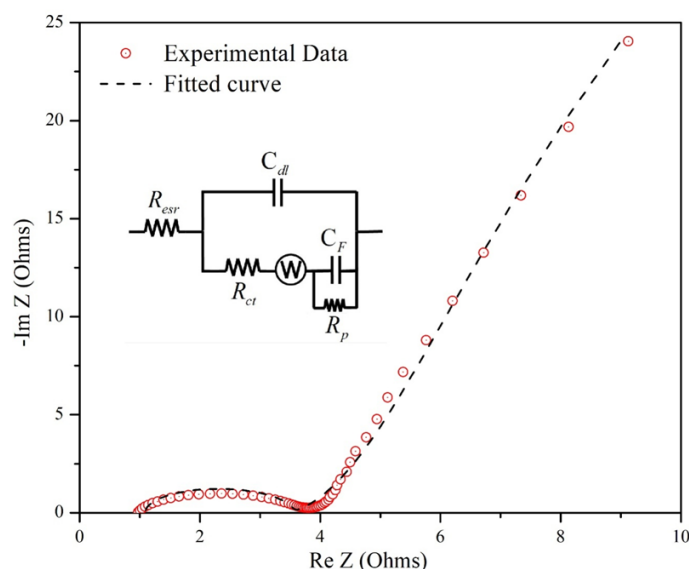

Fig. 9: Nyquist plot and the equivalent circuit for the two electrode test cell

Conclusions

$SnCl_2$ effectively reduces Graphene oxide to Graphene and *in-situ* synthesizing rGO-SnO_2 – PANI composite in one pot. Using the above ternary composite, the supercapacitor with 1M H_2SO_4 electrode showed excellent specific capacitance of 524.2 F/g at a 5 mV/s scan rate, which is a very high value achievable for a two-electrode system. The material showed excellent charge-discharge properties even at a high current density of 1 A/g. The high specific capacitance and high rate capability are attributable to the good charged transfer alone *in-situ* SnO_2 nanocrystallites on the rGO surface. Consequently, the rGO-SnO_2-Polyaniline composite has looked promising as a supercapacitor electrode material and a possible commercial supercapacitor material.

Conflict of interest

There is no conflict of interests regarding the publication of this article

References

1. P. Simon, Y. Gogotsi, Materials for electrochemical capacitors, *Nat. Mater.* 7 (2008) 845–854. https://doi.org/10.1038/nmat2297.
2. Y. Huang, J. Liang, Y. Chen, An Overview of the Applications of Graphene-Based Materials in Supercapacitors, Small. 8 (2012) 1805–1834. https://doi.org/https://doi.org/10.1002/

smll.201102635.
3. A.K. GEIM, K.S. NOVOSELOV, The rise of graphene, in Nanosci. Technol., Co-Published with Macmillan Publishers Ltd, UK, 2009: pp. 11–19. https://doi.org/doi:10.1142/9789814287005_0002.
4. S. Stankovich, D.A. Dikin, G.H.B. Dommett,

K.M. Kohlhaas, E.J. Zimney, E.A. Stach, R.D. Piner, S.T. Nguyen, R.S. Ruoff, Graphene-based composite materials, *Nature.* 442 (2006) 282–286. https://doi.org/10.1038/nature04969.

5.   M.D. Stoller, S. Park, Y. Zhu, J. An, R.S. Ruoff, Graphene-Based Ultracapacitors*, Nano Lett.* 8 (2008) 3498–3502. https://doi.org/10.1021/nl802558y.

6.   B. Varshney, M.J. Siddiqui, A.H. Anwer, M.Z. Khan, F. Ahmed, A. Aljaafari, H.H. Hammud, A. Azam, Synthesis of mesoporous SnO_2/NiO nanocomposite using modified sol-gel method and its electrochemical performance as electrode material for supercapacitors, *Sci. Rep*. 10 (2020) 11032. https://doi.org/10.1038/s41598-020-67990-8.

7.   R. Liang, H. Cao, D. Qian, J. Zhang, M. Qu, Designed synthesis of SnO_2-polyaniline-reduced graphene oxide nanocomposites as an anode material for lithium-ion batteries, *J. Mater. Chem*. 21 (2011) 17654–17657. https://doi.org/10.1039/C1JM13934G.

8.   X. Liu, X. Zhong, Z. Yang, F. Pan, L. Gu, Y. Yu, Gram-Scale Synthesis of Graphene-Mesoporous SnO_2 Composite as Anode for Lithium-ion Batteries, *Electrochim. Acta*. 152 (2015) 178–186. https://doi.org/https://doi.org/10.1016/j.electacta.2014.11.100.

9.   K. Gopalakrishnan, S. Sultan, A. Govindaraj, C.N.R. Rao, Supercapacitors based on composites of PANI with nanosheets of nitrogen-doped RGO, BC1.5N, MoS2 and WS2, *Nano Energy*. 12 (2015) 52–58. https://doi.org/https://doi.org/10.1016/j.nanoen.2014.12.005.

10. X. Xia, Q. Hao, W. Lei, W. Wang, H. Wang, X. Wang, Reduced-graphene oxide/molybdenum oxide/polyaniline ternary composite for high energy density supercapacitors: Synthesis and properties, *J. Mater. Chem*. 22 (2012) 8314–8320. https://doi.org/10.1039/C2JM16216D.

11. X. Xia, Q. Hao, W. Lei, W. Wang, D. Sun, X. Wang, Nanostructured ternary composites of graphene/Fe2O3/polyaniline for high-performance supercapacitors, *J. Mater. Chem*. 22 (2012) 16844–16850. https://doi.org/10.1039/C2JM33064D.

12. T. Kshetri, D.T. Tran, D.C. Nguyen, N.H. Kim, K. Lau, J.H. Lee, Ternary graphene-carbon nanofibers-carbon nanotubes structure for hybrid supercapacitor, *Chem. Eng. J*. 380 (2020) 122543. https://doi.org/https://doi.

org/10.1016/j.cej.2019.122543.

13. M. Maher, S. Hassan, K. Shoueir, B. Yousif, M.E.A. Abo-Elsoud, Activated carbon electrode with promising specific capacitance based on potassium bromide redox additive electrolyte for supercapacitor application, *J. Mater. Res. Technol*. 11 (2021) 1232–1244. https://doi.org/https://doi.org/10.1016/j.jmrt.2021.01.080.

14. Y. Fan, H. Chen, Y. Li, D. Cui, Z. Fan, C. Xue, PANI-Co3O4 with excellent specific capacitance as an electrode for supercapacitors, *Ceram. Int.* 47 (2021) 8433–8440. https://doi.org/https://doi.org/10.1016/j.ceramint.2020.11.208.

15. C. Douard, L. Athouël, D. Brown, O. Crosnier, G. Rebmann, O. Schilling, T. Brousse, Electrode Design for MnO2-Based Aqueous Electrochemical Capacitors: Influence of Porosity and Mass Loading, *Mater.* . 14 (2021). https://doi.org/10.3390/ma14112990.

16. G. Ni, F. Qin, Z. Guo, J. Wang, W. Shen, Nitrogen-doped asphaltene-based porous carbon fibers as supercapacitor electrode material with high specific capacitance, *Electrochim. Acta.* 330 (2020) 135270. https://doi.org/https://doi.org/10.1016/j.electacta.2019.135270.

17. V. Khomenko, E. Frackowiak, F. Béguin, Determination of the specific capacitance of conducting polymer/nanotubes composite electrodes using different cell configurations, Electrochim. *Acta*. 50 (2005) 2499–2506. https://doi.org/https://doi.org/10.1016/j.electacta.2004.10.078.

18. S. Wu, Y. Zhu, Highly densified carbon electrode materials towards practical supercapacitor devices, *Sci. China Mater.* 60 (2017) 25–38. https://doi.org/10.1007/s40843-016-5109-4.

19. M. Sajjad, Y. Khan, W. Lu, One-pot Synthesis of 2D SnS2 Nanorods with High Energy Density and Long Term Stability for High-Performance Hybrid Supercapacitor, J. Energy Storage. 35 (2021) 102336. https://doi.org/https://doi.org/10.1016/j.est.2021.102336.

20. M.D. Stoller, R.S. Ruoff, Best practice methods for determining an electrode material's performance for ultracapacitors, *Energy Environ. Sci.* 3 (2010) 1294–1301. https://doi.org/10.1039/C0EE00074D.

21. V.C. Jayawardena, D.R. Jayasundara, G. Amaratunga, V. Jayaweera, Method for the synthesis of graphene oxide, (2019).

22. I.R.M. Kottegoda, X. Gao, L.D.C. Nayanajith,

C.H. Manorathne, J. Wang, J.-Z. Wang, H.-K. Liu, Y. Gofer, Comparison of Few-layer Graphene Prepared from Natural Graphite through Fast Synthesis Approach, *J. Mater. Sci. Technol*. 31 (2015) 907–912. https://doi.org/https://doi.org/10.1016/j.jmst.2015.07.014.

23. M. Jayaweera, R.C.L. De Silva, I.R.M. Kottegoda, S.R.D. Rosa, Synthesis, characterization and ethanol vapor sensing performance of SnO2/Graphene composite film, Sri Lankan *J. Phys.* 15 (2015).

24. P. Ghasemipour, M. Fattahi, B. Rasekh, F. Yazdian, Developing the Ternary ZnO Doped MoS2 Nanostructures Grafted on CNT and Reduced Graphene Oxide (RGO) for Photocatalytic Degradation of Aniline, *Sci. Rep.* 10 (2020) 4414. https://doi.org/10.1038/s41598-020-61367-7.

25. A. Debataraja, D.W. Zulhendri, B. Yuliarto, Nugraha, Hiskia, B. Sunendar, Investigation of Nanostructured SnO2 Synthesized with Polyol Technique for CO Gas Sensor Applications, *Procedia Eng.* 170 (2017) 60–64. https://doi.org/https://doi.org/10.1016/j.proeng.2017.03.011.

26. S.P. Kim, M.Y. Choi, H.C. Choi, Photocatalytic activity of SnO2 nanoparticles in methylene blue degradation, *Mater. Res. Bull.* 74 (2016) 85–89. https://doi.org/https://doi.org/10.1016/j.materresbull.2015.10.024.

27. Y. Zhang, J. Liu, Y. Zhang, J. Liu, Y. Duan, Facile synthesis of hierarchical nanocomposites of aligned polyaniline nanorods on reduced graphene oxide nanosheets for microwave absorbing materials, *RSC Adv.* 7 (2017) 54031–54038. https://doi.org/10.1039/C7RA08794B.

28. L.Z. Liu, T.H. Li, X.L. Wu, J.C. Shen, P.K. Chu, Identification of oxygen vacancy types from Raman spectra of SnO2 nanocrystals, *J. Raman Spectrosc.* 43 (2012) 1423–1426. https://doi.org/https://doi.org/10.1002/jrs.4078.

29. Z. Morávková, P. Bober, Writing in a Polyaniline Film with Laser Beam and Stability of the Record: A Raman Spectroscopy Study, *Int. J. Polym. Sci.* 2018 (2018) 1797216. https://doi.org/10.1155/2018/1797216.

30. R.F. Martinez-Gazoni, M.W. Allen, R.J. Reeves, Conductivity and transparency limits of Sb-doped $\mathrm{Sn}{\mathrm{O}}_{2}$ grown by molecular beam epitaxy, *Phys. Rev*. B. 98 (2018) 155308. https://doi.org/10.1103/*PhysRevB.*98.155308.